International Journal of Nanomedicine

Dovepress
open access to scientific and medical research

Open Access Full Text Article

ORIGINAL RESEARCH

PDADMAC/Alginate-Coated Gold Nanorod For Eradication of Staphylococcus Aureus Biofilms

Malarmugila Manimaran[1,*], Yin Yin Teo[2], James Chen Yong Kah[3], Adilet Beishenaliev[1], Yean Leng Loke[2], Yiing Yee Foo[1], Shiow-Fern Ng[4], Chin Fei Chee[5], Sek Peng Chin[6], Farid Nazer Faruqu[1], Chia-Yu Chang[7], Misni Misran[2], Lip Yong Chung[6], Bey Fen Leo[8,*], Shih-Hwa Chiou[9,10], Chia-Ching Chang[7,11–13], Sun Tee Tay[14], Lik Voon Kiew[1,7]

[1]Department of Pharmacology, Faculty of Medicine, Universiti Malaya, Kuala Lumpur, Malaysia; [2]Department of Chemistry, Faculty of Science, Universiti Malaya, Kuala Lumpur, Malaysia; [3]Department of Biomedical Engineering, College of Design and Engineering, National University of Singapore, Singapore, Singapore; [4]Centre for Drug Delivery Technology and Vaccine, Faculty of Pharmacy, Universiti Kebangsaan Malaysia, Kuala Lumpur, Malaysia; [5]Nanotechnology Catalysis Research Centre, Universiti Malaya, Kuala Lumpur, Malaysia; [6]Department of Pharmaceutical Chemistry, Faculty of Pharmacy, Universiti Malaya, Kuala Lumpur, Malaysia; [7]Department of Biological Science and Technology, National Yang Ming Chiao Tung University, Hsinchu, Taiwan, Republic of China; [8]Department of Molecular Medicine, Faculty of Medicine, Universiti Malaya, Kuala Lumpur, Malaysia; [9]Department of Medical Research, Taipei Veterans General Hospital, Taipei, Taiwan, Republic of China; [10]Institute of Pharmacology, National Yang Ming Chiao Tung University, Taipei, Taiwan, Republic of China; [11]Department of Electrophysics, National Yang Ming Chiao Tung University, Hsinchu, Taiwan, Republic of China; [12]Center for Intelligent Drug Systems and Smart Bio-devices, National Yang Ming Chiao Tung University, Hsinchu, Taiwan, Republic of China; [13]Institute of Physics, Academia Sinica, Nankang, Taipei, Taiwan, Republic of China; [14]Department of Medical Microbiology, Faculty of Medicine, Universiti Malaya, Kuala Lumpur, Malaysia

*These authors contributed equally to this work

Correspondence: Chia-Ching Chang; Lik Voon Kiew, Email ccchang01@nycu.edu.tw; lvkiew@um.edu.my

Introduction: Over 75% of clinical microbiological infections are caused by bacterial biofilms that grow on wounds or implantable medical devices. This work describes the development of a new poly(diallyldimethylammonium chloride) (PDADMAC)/alginate-coated gold nanorod (GNR/Alg/PDADMAC) that effectively disintegrates the biofilms of *Staphylococcus aureus* (*S. aureus*), a prominent pathogen responsible for hospital-acquired infections.

Methods: GNR was synthesised via seed-mediated growth method, and the resulting nanoparticles were coated first with Alg and then PDADMAC. FTIR, zeta potential, transmission electron microscopy, and UV–Vis spectrophotometry analysis were performed to characterise the nanoparticles. The efficacy and speed of the non-coated GNR and GNR/Alg/PDADMAC in disintegrating *S. aureus*-preformed biofilms, as well as their in vitro biocompatibility (L929 murine fibroblast) were then studied.

Results: The synthesised GNR/Alg/PDADMAC (mean length: 55.71 ± 1.15 nm, mean width: 23.70 ± 1.13 nm, aspect ratio: 2.35) was biocompatible and potent in eradicating preformed biofilms of methicillin-resistant (MRSA) and methicillin-susceptible *S. aureus* (MSSA) when compared to triclosan, an antiseptic used for disinfecting *S. aureus* colonisation on abiotic surfaces in the hospital. The minimum biofilm eradication concentrations of GNR/Alg/PDADMAC ($MBEC_{50}$ for MRSA biofilm = 0.029 nM; $MBEC_{50}$ for MSSA biofilm = 0.032 nM) were significantly lower than those of triclosan ($MBEC_{50}$ for MRSA biofilm = 10,784 nM; $MBEC_{50}$ for MRSA biofilm 5967 nM). Moreover, GNR/Alg/PDADMAC was effective in eradicating 50% of MRSA and MSSA biofilms within 17 min when used at a low concentration (0.15 nM), similar to triclosan at a much higher concentration (50 μM). Disintegration of MRSA and MSSA biofilms was confirmed by field emission scanning electron microscopy and confocal laser scanning microscopy.

Conclusion: These findings support the potential application of GNR/Alg/PDADMAC as an alternative agent to conventional antiseptics and antibiotics for the eradication of medically important MRSA and MSSA biofilms.

Keywords: biofilm, gold nanorod, *S. aureus*, PDADMAC, MRSA, MSSA

Introduction

Staphylococcus aureus is a gram-positive bacterial pathogen responsible for a wide variety of community and hospital-acquired infections. This organism has developed resistance to multiple antibiotics owing to its extensive and injudicious antibiotic use.

Received: 28 November 2023
Accepted: 5 April 2024
Published: 23 April 2024

Methicillin-resistant *S. aureus* (MRSA) outbreaks in hospitalised patients have been consistently reported worldwide, including in high-income nations. In the European Union (EU), these infections are projected to affect more than 150,000 individuals annually.[1] MRSA is common in almost all healthcare institutions in Asia and poses a significant burden.[2]

S. aureus's recalcitrance and the rapid development of resistance to antibiotics correlate with biofilm formation at the site of infection.[3] Biofilms are polymeric matrices that house multicellular microbial colonies. They are resistant to external stresses and can disseminate to new surfaces.[4,5] Biofilms contribute to over 75% of clinical microbial infections[4,6] and more than 80% of all infections in humans,[7] notably osteomyelitis, otitis media, periodontitis, and infections of the surgical site, urinary tract, and respiratory tract.[8]

Biofilms protect bacteria by (i) blocking the penetration of antibiotics such as beta-lactams, aminoglycosides, and glycopeptides via their dense exopolysaccharides and extracellular DNA matrices;[9–11] (ii) degrading antibiotics or affecting antibiotic efficiencies via their harsh microenvironment (eg, acidic pH and hypoxia);[12] and (iii) decreasing the metabolic activity of the resident bacteria, thereby reducing bacterial susceptibility to anti-metabolic/anti-replicative actions of antibiotics.[13,14] This has encouraged the development of antibiotic-resistant bacteria in biofilm.[15,16] As a result, a higher minimum biofilm eradication concentration (MBEC, approximately 10–10,000 times higher) of antibiotics is required to destroy biofilm-associated bacteria than planktonic cells.[17] Nevertheless, the administration of such a high antibiotic dose to patients is not feasible owing to the adverse effects of antibiotics and renal and hepatic clearance limitations.[18] Additionally, excessive antibiotic use may result in higher treatment costs and emergence of multidrug-resistant bacteria.[19]

The use of antibiotics to treat *S. aureus* biofilm-associated infections is reportedly ineffective. For example, Olson et al reported that tetracycline, streptomycin, enrofloxacin, oxytetracycline, erythromycin, penicillin G, cloxacillin, gentamicin, ceftiofur, tilmicosin, trimethoprim-sulphadoxine, and ampicillin were effective in eradicating planktonic cultures of *S. aureus* but not biofilms.[20] Furthermore, vancomycin, the most commonly administered drug for MRSA infection,[21] was ineffective in killing both MRSA and methicillin-susceptible *S. aureus* (MSSA) cells within the biofilm.[22] Although synergistic antibiotic combinations such as rifampicin-fosfomycin, vancomycin-rifampin, and daptomycin-rifampin have been reported to be effective against staphylococcal biofilms in vitro, their in vivo efficiencies have yet to be determined.[23–25] Therefore, novel anti-biofilm therapeutics that can effectively disrupt biofilm with minimal adverse effects on patients and the development of antibiotic-resistance would be sought.

Over the past decade, the use of metallic nanoparticles to inhibit biofilm formation has been increasingly explored. Successful examples include the use of copper(II) oxide (CuO) to inhibit biofilms of oral bacteria (inhibitory concentration, IC_{50} = 50 μg/mL)[26] and MRSA and *Escherichia coli* (IC_{50} = 30–35 μg/mL),[27] zinc oxide (ZnO) to inhibit biofilms of *Streptococcus pneumoniae* (IC_{50} = 12 μg/mL) and uropathogenic *E. coli* (IC_{50} = 2791 μg/mL),[28] magnesium oxide to inhibit biofilms of *Staphylococcus epidermidis* (IC_{50} = 1600 μg/mL),[29] *Klebsiella pneumoniae* (IC_{50} = 125 μg/mL), *E. coli* (IC_{50} = 250 μg/mL), and *S. aureus* (IC_{50} = 500 μg/mL),[30] and titanium dioxide (TiO_2) to partially inhibit *Pseudomonas aeruginosa* (IC_{50} = 31 μg/mL, 30% inhibition),[31] *E. coli* and *Bacillus subtilis* (both IC_{50} = 15 μg/mL, 40–50% inhibition).[32] The anti-biofilm properties of these nanoparticles (NPs) are attributed to the release of toxic metal ions (eg, CuO and ZnO) to impede bacterial growth and biofilm production,[26,27,33] or the generation of reactive oxygen species (eg, TiO_2) to oxidise the lipid cell wall membrane of biofilm bacteria.[34,35] However, a relatively high concentration of NPs is often required to achieve a satisfactory anti-biofilm efficacy. Thus, there are significant concerns regarding host cytotoxicity at high NP doses.[36,37]

Physical disintegration of the biofilm structure may assist in reducing the bacterial load at biofilm-infected sites and enhancing the penetration and performance of other antimicrobials in synergistic therapies.[38] Previously, polyelectrolytes, particularly polycations, were demonstrated to interact with the negatively charged bacterial cell wall components and biofilm,[39] thus compromising cell wall integrity and biofilm structure and causing their disintegration. This suggests the possible use of cationic polyelectrolytes for antibacterial and anti-biofilm applications. However, while cationic polyelectrolytes have been frequently investigated as antibacterial coatings,[40] their potential as coatings on biocompatible nanoparticles for biofilm disintegration has been relatively less explored.

In this study, we synthesised and characterised a new biocompatible cationic poly(diallyldimethylammonium chloride) (PDADMAC)/alginate-coated gold nanorod (GNR/Alg/PDADMAC) and investigated its in vitro efficiency in disintegrating biofilms of clinically significant bacteria (MSSA and MRSA).

Materials and Methods

Materials

Ascorbic acids, thiazolyl blue tetrazolium bromide (MTT) and cetyltrimethylammonium bromide (CTAB), were purchased from BioBasic (Canada). Hydrogen tetrachloroaurate(III) ($HAuCl_4 \cdot 3H_2O$) and phosphate-buffered saline (PBS) tablets were purchased from Sigma-Aldrich (Germany). Dimethyl sulfoxide (DMSO) and sodium borohydride ($NaBH_4$) were purchased from Merck (Germany). Sodium alginate (300–400 mPa·s) was obtained from Chemiz (Malaysia). Triclosan, and poly(diallyldimethylammonium chloride) PDADMAC (20 wt. % in H_2O) were obtained from Sigma-Aldrich (USA). Muller Hinton Broth (MHB) was purchased from BD Difco™ (USA). Glucose (1%) was obtained from Systerm (Malaysia). Silver nitrate ($AgNO_3$) was purchased from Bendosen (Malaysia). Dulbecco's modified Eagle medium (DMEM) was obtained from Nacalai Tesque (Kyoto, Japan). Unless otherwise specified, all the reagents were prepared using Milli-Q ultrapure water.

Synthesis of Gold Nanorod (GNR)

With minor adjustments, the seed-mediated growth technique reported by Nikoobakht et al was used to synthesise GNR.[41] The seed solution was prepared by mixing CTAB (5 mL, 0.2 M), $HAuCl_4 \cdot 3H_2O$ (5 mL, 0.5 mM), and ice-cold $NaBH_4$ (600 µL, 10 mM) with vigorous stirring (800 rpm) at 35°C for 2 min. The seed solution was left undisturbed. The growth solution was then prepared by combining CTAB (5 mL, 0.2 M), $HAuCl_4 \cdot 3H_2O$ (5 mL, 1.0 mM) with a freshly prepared ice-cold $AgNO_3$ (50 µL, 10 mM), ascorbic acid (85 µL, 78.8 mM), and the seed solution (12 µL) and continuously stirred at 700 rpm for 10 s. The growth solution was left undisturbed in the dark for 3 h. The resulting GNR were centrifuged (at 4700× g for 20 minutes), washed twice with ultrapure water, and stored in the dark at room temperature (25°C) before further use.

Synthesis of Alginate-Coated GNR (GNR/Alg) and PDADMAC/Alginate-Coated GNR (GNR/Alg/PDADMAC)

For the synthesis of GNR/Alg, GNRs were coated with alginate by adding a 5 mg/mL alginate solution in ultrapure water to the GNR solution at a 1:1 volume ratio. The mixture was shaken for 4 h in a thermoshaker (750 rpm, 25°C). Next, the GNR/Alg solution was centrifuged at 4700 × g for 30 min to remove excess alginate and resuspended in a 1 mM sodium chloride solution (NaCl). To synthesise GNR/Alg/PDADMAC, a 5 mg/mL PDADMAC solution was prepared in 1 mM NaCl. It was then mixed with GNR/Alg in a 1:1 volume ratio and shaken for 4 h, followed by washing and resuspension in 1 mM NaCl. Both GNR/Alg and GNR/Alg/PDADMAC were stored at room temperature (25°C) before use.

Physicochemical Characterisation of GNR/Alg/PDADMAC

The UV–Vis light absorption spectra of GNR, GNR/Alg, and GNR/Alg/PDADMAC were obtained using a UV–Vis spectrophotometry[42] (NanoDrop 2000c Spectrophotometer, Thermo Scientific, USA). Zeta potential measurements were performed using a Zetasizer (NanoZS, Malvern Instruments, UK) at 25°C. The stability of GNR/Alg/PDADMAC over time (4 weeks) in phosphate-buffered saline (PBS) at 25°C was observed using UV–Vis spectrophotometry and zeta potential measurements. The polyelectrolyte coating stability of GNR/Alg/PDADMAC was monitored at pH 4–8 using zeta-potential measurements. The pH of the samples was adjusted using 0.1M hydrochloric acid and 0.1M sodium hydroxide. FTIR analysis was performed using a Spectrum 400 (Perkin Elmer, USA) with a scanning range of 500–4000 cm^{-1} and a resolution of 2 cm^{-1}.

The morphology of GNR/Alg/PDADMAC was observed using TEM at 4000× magnification. Samples for TEM were prepared by placing 10 µL of 0.15 nM GNR/Alg/PDADMAC dispersion onto carbon-coated copper grids and allowed to adsorb for 10 min, followed by the addition of 10 µL of 2% phosphotungstic acid (PTA) aqueous solution as negative staining was added to the carbon surface.[43] After 5 min, the grid was allowed to air dry after the excess staining agent was removed by contact with the edge of a piece of filter paper before being viewed under TEM (LEO LIBRA 120, Carl Zeiss, Germany).

Biofilm Eradication Assay

Two commercially purchased *S. aureus* strains, MSSA ATCC 29213 and MRSA ATCC 43300, were used in this study. The ability of GNR and GNR/Alg/PDADMAC to destroy *S. aureus*-preformed biofilms was tested, as described previously.[44] All experiments were performed in triplicate on pre-sterilised flat-bottom polystyrene 96-well microtitre plates. Briefly, an overnight-grown *S. aureus* broth culture, adjusted to a cell density of 0.5, McFarland turbidity standard using a spectrophotometer (GENESYS™ 20, Thermo Fisher Scientific Inc., USA), was diluted to 2×10^6 colony forming units (cfu)/mL with MHB supplemented with 1% glucose (growth media) before being dispensed into microtitre wells. Next, 100 µL of diluted cells were added to the wells of microtitre plates containing 100 µL of growth media. The final cell density of *S. aureus* was 1×10^6 cfu/mL. The growth control (untreated biofilm) was prepared by adding 100 µL of bacterial suspension to 100 µL of growth media. Sterile control wells were prepared by adding 200 µL of growth medium. Finally, the prepared microtitre plate was incubated in a shaking incubator (200 rpm) for 4 h at 37°C and rinsed twice with 200 µL PBS. The rinsed wells were then filled with the same volume of growth medium and incubated for 24 h at 37°C in a shaking incubator for mature biofilm development. After 24 h of incubation, the biofilm-coated wells were washed three times with 200 µL sterile PBS. Next, ascending concentrations (after 10-fold serial dilution) of GNR and GNR/Alg/PDADMAC (concentration range: 0.02–0.15 nM of NPs) and positive control (triclosan, concentration range: $1.0 \times 10^3 - 1.0 \times 10^5$ nM) were added to the respective wells and incubated at 37°C for an additional 24 h. Triclosan was chosen as the positive control in this biofilm eradication assay because it functions as an antiseptic and has been found to inhibit and disperse biofilms owing to its broad-spectrum antibacterial action.[45] Additionally, it has been applied topically as a surface coating to prevent infections caused by biofilms.[46]

A crystal violet (CV) assay was performed.[47] First, the contents of all microtitre wells were aspirated and washed three times with 200 µL sterile PBS. The microtitre plates were then air-dried in an inverted position, followed by fixation of the biofilm in each microtitre well with 150 µL 95% (v/v) methanol for 15 min. Methanol was then decanted, and the microtitre plates were air-dried in an inverted position. The biofilms in the wells were subsequently stained with 150 µL of 0.1% (v/v) CV solution for 15 min. The wells were then washed three times with ultrapure water and air-dried. Finally, the CV stain left behind in the wells was solubilised using 150 µL of 33% (v/v) glacial acetic acid, and the optical absorbance of the resultant solution was measured at 570 nm using a microplate reader (Tecan Austria GmbH, Austria). The percentage of biofilm eradication was calculated by comparison with the growth control using the formula described in the Supplementary Section.

Biofilm Time Point Assay

The 24-hour grown biofilms were washed three times with 200 µL of sterile PBS, as mentioned in the previous biofilm eradication assay, and 0.03 nM ($MBEC_{50}$) of GNR/Alg/PDADMAC was added to the biofilm-coated wells. The growth control, positive control and treated plates were incubated at 37°C for specific time point intervals (1, 2, 5, 10, 15, 20, 25, 30 and 60 minutes). Each plate was removed from the incubator after reaching the indicated time points, washed, and stained for CV assay, as described in the biofilm eradication assay protocol (Biofilm Eradication Assay). The CV-stained plates were observed under a light microscope.

Field Emission Scanning Electron Microscopy (FESEM)

S. aureus cultures cultivated overnight were diluted in the growth medium to obtain 10^6 cfu/mL *S. aureus*. Biofilm cultures were prepared on glass coverslips in which a glass slide was positioned in the middle of each well (6-well plate). The plates were incubated at 37°C for 24 h to allow biofilm growth on the slides. Then, GNR/Alg/PDADMAC was added to each well at 0.03 nM and incubated at 37°C for 24 h. The biofilm cultures (growth control and GNR/Alg/PDADMAC-treated) were treated with 2% (w/v) osmium tetroxide for 1 h after overnight fixation with 4% glutaraldehyde in a cacodylate buffer. The cultures were then dried in various solutions of ethanol (10–100%), ethanol: acetone blends (3:1, 1:1, and 1:3), and acetone. Each sample was mounted on an aluminium stub and coated with gold (Bio-Rad E5100 Series 11, USA) for viewing under the FESEM FEI Quanta 450 FEG (USA) after drying in CO_2 (CPD 7501, Polaron, UK).

Confocal Laser Scanning Microscopy (CLSM)

For CLSM imaging, biofilms were cultivated on glass coverslips in polystyrene 24-microtiter well plates. Microscopic imaging was performed on *S. aureus*-preformed biofilms incubated with GNR/Alg/PDADMAC (0.03 nM for 24 h) and on those without NP treatment (growth control). The biofilms were stained using the LIVE/DEAD BacLight Bacterial Viability Kit (Invitrogen, USA) in the dark for 15 min and rinsed with sterile PBS. Images of the biofilms were acquired using an inverted Leica SP5 Confocal Scanning Laser Microscope (Leica Microsystems GmbH, Germany), excited with 488 and 561 nm lasers, and analysed using the LAS AF software (Leica Microsystems, Germany).

In vitro Biocompatibility

The in vitro biocompatibility of GNR/Alg/PDADMAC and the positive control (triclosan) was assessed using MTT assays.[48] Murine fibroblast cells (L929) from a commercial source ATCC were used as a model and seeded into 96-well plates (6000 cells per well) containing DMEM supplemented with 1% penicillin/streptomycin and 10% fetal bovine serum and grown overnight in a humidified 5% CO_2 incubator at 37°C. Subsequently, a series concentration of GNR/Alg/PDADMAC solution (0.0037–0.3 nM; or 0.90–73.60 µg/mL gold equivalent) and triclosan (5.0×10^3, 1.0×10^4, 2.0×10^4, 4.0×10^4, $8.0 \times 10,^4$ and 1.0×10^5 nM, equivalent to 3–100 µg/mL by mass) were added to the cells. After incubation for 24 h, 20 µL MTT solution (5 mg/mL) was added to each well and incubated for another 4 h. To dissolve the resulting formazan crystals, 200 mL of DMSO was added to each well after removing all the media. The absorbance was measured at 570 nm using a microplate reader (Plate Chameleon V, Finland).

Statistical Analysis

All statistical analyses were performed using GraphPad Prism 10.2 software (Prism, USA). Statistical analysis methods used include Welch's *t*-test and 2-way ANOVA – Bonferroni's multiple comparisons test, with a probability of $p < 0.05$ considered statistically significant.

Results

UV–Vis Spectrophotometry

UV–Vis spectra of the non-coated gold nanorods (GNR), alginate-coated gold nanorods (GNR/Alg) and PDADMAC/alginate-coated gold nanorods (GNR/Alg/PDADMAC) are shown in Figure 1A. GNRs exhibited two plasmonic resonances corresponding to transverse surface plasmon resonance (TSPR) at 515 ± 1.15 nm and longitudinal surface plasmon resonance (LSPR) at 655 ± 0.58 nm due to anisotropic configuration.[49]

Alginate was then coated onto the GNR as an interfacial layer between the GNR and PDADMAC coating. The alginate coating resulted in a slight shift in both the TSPR (to 517 ± 0.58 nm) and LSPR (to 661 ± 1.00 nm) band maxima, which might be explained by an increase in the local dielectric function caused by the presence of alginate polymer.[50] The absorbance bands of GNR/Alg/PDADMAC showed a further red-shift after coating with PDADMAC.[51] The TSPR of GNR/Alg/PDADMAC was 519 ± 1.00 nm, and the LSR was 669 ± 1.15 nm. The minimal alterations in the maximum absorbance wavelength of GNR after coating with alginate and PDADMAC, along with the absence of the broadening of absorbance bands, further indicated the physical stability of both GNR/Alg and GNR/Alg/PDADMAC, with no agglomeration post-coating (Figure 1A). The concentration of GNR was estimated from the UV–Vis spectra using a technique described in a previous study[41] (the formula is indicated in the Supplementary Materials).

The physical stability of GNR/Alg/PDADMAC stored at room temperature (25°C) over four weeks in PBS was monitored and characterised using UV–Vis spectrophotometry. The GNR/Alg/PDADMAC showed TSPR at ~514 ± 0.58 nm and LSPR at ~664 ± 1.15 nm. A minimal shift in the absorbance bands (± 10 nm) was observed even after four weeks of storage. Furthermore, no significant broadening of the bands was observed, indicating no agglomeration or changes in shape[52] of GNR/Alg/PDADMAC for up to 4 weeks of storage at room temperature (Figure 1B).

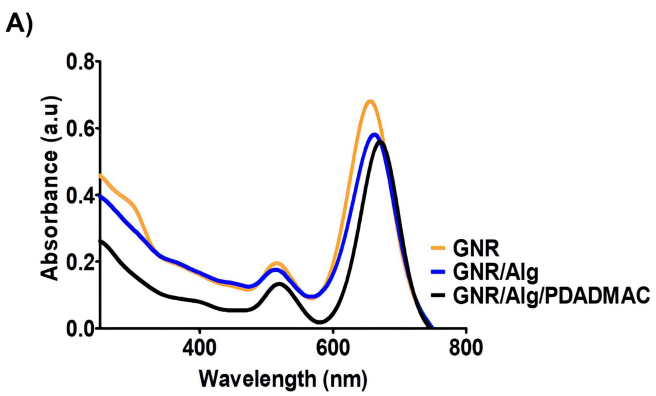

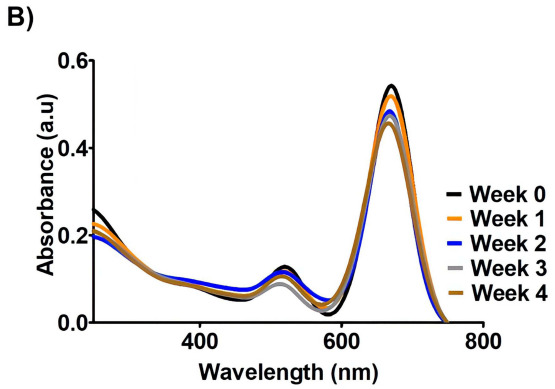

Sample	Wavelength (nm)	
	TSPR	LSPR
GNR	515 ± 1.15	655 ± 0.58
GNR/Alg	517 ± 0.58	661 ± 1.00
GNR/Alg/PDADMAC	519 ± 1.00	669 ± 1.15

GNR/Alg/PDADMAC	Wavelength (nm)	
	TSPR	LSPR
Week 0	519 ± 1.00	669 ± 1.15
Week 1	518 ± 0.58	668 ± 1.15
Week 2	517 ± 1.53	667 ± 0.58
Week 3	515 ± 0.58	665 ± 0.58
Week 4	514 ± 0.58	664 ± 1.15

Figure 1 (**A**) UV-Vis Spectra of non-coated gold nanorod (GNR), alginate-coated gold nanorod (GNR/Alg) and PDADMAC/alginate-coated gold nanorod (GNR/Alg/PDADMAC). (**B**) No significant change in the UV-Vis spectra of GNR/Alg/PDADMAC after 4 weeks of incubation in PBS at 25°C, suggesting the stability of GNR/Alg/PDADMAC in the aqueous environment over time. Data are represented as mean ± SD (n = 3).

Zeta Potential Measurement

The zeta potential value of GNR changed from +27.33 ± 1.94 to −58.27 ± 2.40 mV following the coating of alginate onto its surface, while the value reversed to +42.80 ± 0.61 mV following the subsequent PDADMAC coating (Figure 2A). Charge reversal indicates the successful deposition of polyelectrolytes on the surface of the GNR, with cationic PDADMAC as the terminal layer.

The stability of the GNR/Alg/PDADMAC was evaluated on PBS at room temperature. GNR/Alg/PDADMAC remained stable at pH 7 throughout the four weeks of observation, with minimal changes in zeta potential (Figure 2B). The results indicated that GNR/Alg/PDADMAC was physically stable at room temperature for at least four weeks and would benefit medical use.

The stability of the GNR/Alg/PDADMAC polyelectrolyte coating was examined in microenvironments of different pH values (4–8). The zeta potential of GNR/Alg/PDADMAC remained positive across all tested pH values (Figure 2C), suggesting the good stability of the polyelectrolyte coating. A reduction of GNR/Alg/PDADMAC zeta potential following the increase of the microenvironment's pH (from +61.70 ± 4.50 mV at pH 4 to +22.10 ± 2.20 mV at pH 8) was observed. This is probably due to the preferential adsorption of hydroxide ions from the medium onto the GNR/Alg/PDADMAC surfaces. In contrast, excessive hydronium ion concentration in an acidic solution causes hydronium ions to adsorb onto the polymer interface, increasing the zeta potential of the GNR/Alg/PDADMAC surfaces.[53] Such a strong positive charge of GNR/Alg/PDADMAC within the acidic biofilm microenvironment may facilitate deep penetration of GNR/Alg/PDADMAC into biofilms, encourage the attachment of GNR/Alg/PDADMAC to biofilm cells, and contribute to the destruction of biofilms and bacteria cells.[54]

FTIR

In the FTIR analysis, the strong absorptions at 2918 and 2850 cm^{-1} in the GNR were caused by the C–H stretching vibration of the methyl and methylene groups of CTAB. In both the GNR/Alg and GNR/Alg/PDADMAC samples, a solid and wide band at 3445 cm^{-1} (owing to the stretching vibration of hydroxyl groups) was observed, whereas the intensity of the signals representing CTAB was weak. The alginate coating of GNR was confirmed by the appearance of O–H, asymmetric/symmetric COO–, and C–O stretching vibrations of alginate at 3345, 1595, 1460 and 1020 cm^{-1},

A)

Sample	Zeta potential (mV)
GNR	+ 27.33 ± 1.94
GNR/Alg	- 58.27 ± 2.40
GNR/Alg/PDADMAC	+ 42.80 ± 0.61

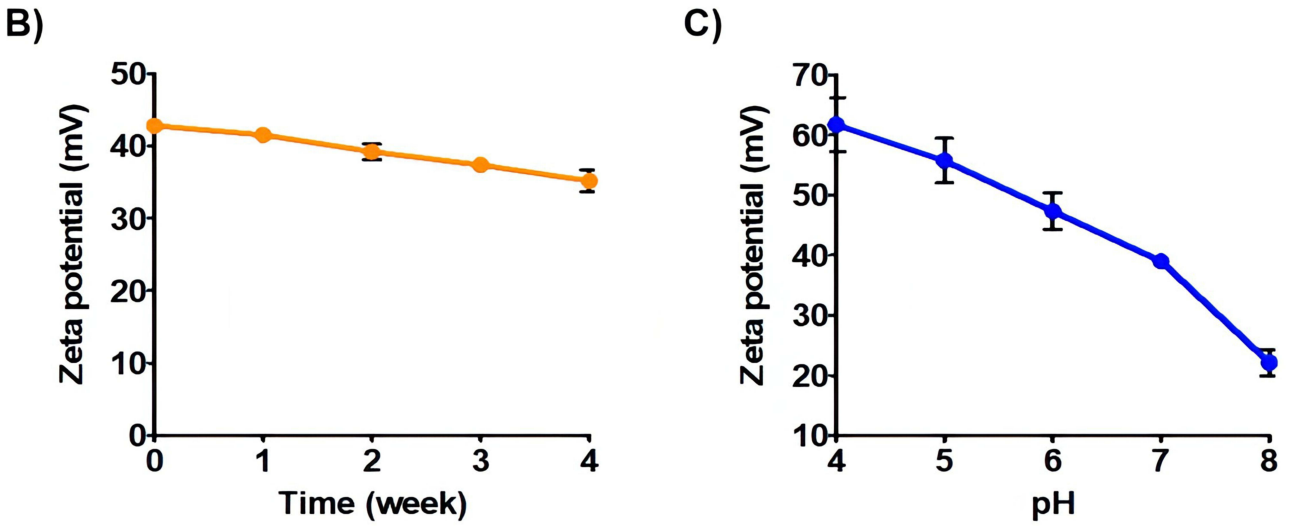

Figure 2 (**A**) Zeta potential values of non-coated gold nanorod (GNR), alginate-coated gold nanorod (GNR/Alg) and PDADMAC/alginate-coated gold nanorod (GNR/Alg/PDADMAC). (**B**) Minor decrease in the zeta potential value of PDADMAC/alginate-coated gold nanorod (GNR/Alg/PDADMAC) after 4 weeks of incubation in PBS at 25°C, suggesting the physical stability of GNR/Alg/PDADMAC over time. (**C**) The PDADMAC/alginate-coated gold nanorod (GNR/Alg/PDADMAC) remain positively charged in different pH ranges. Data are represented as mean ± SD (n = 3).

respectively. The appearance of $–CH_3$, $–CH_2$ and –CN stretching vibrations at 1465, 2900 and 2100 cm^{-1}, respectively, confirmed the presence of the PDADMAC coating on the GNR/Alg (Figure 3).

TEM

The synthesised GNR and GNR/Alg/PDADMAC micrographs (Figure 4) obtained by TEM exhibited rod-like shapes. GNR had a mean length of 55.71 ± 1.15 nm, width of 23.70 ± 1.13 nm, and aspect ratio of 2.35 (n = 100). The polyelectrolyte coating on the GNR surface was also observed in the TEM micrograph as a faint layer surrounding the GNR via negative staining with 2% PTA. The coating thickness was calculated to be 2.55 ± 0.67 nm (n = 100). This result is consistent with the reported polyelectrolyte (PDADMAC) coating thicknesses of 2–3 nm.[55,56]

Biofilm Eradication Assay

GNR/Alg/PDADMAC exhibited dose-dependent biofilm eradication activity, eradicating approximately 86% of MRSA biofilms and 93% of MSSA biofilms at a sub-nanomolar concentration (0.15 nM) (Figures 5 and 6). Such biofilm eradication efficiencies were comparable to those of triclosan (treatment control) but attained a 333,333-fold lower concentration than triclosan (maximum biofilm eradication estimated for both MRSA biofilm (87% eradication) and MSSA biofilm (89% eradication) at 50 μM triclosan).

With regard to biofilm eradication potency, GNR/Alg/PDADMAC exhibited 371,862-fold higher potency in the eradication of MRSA biofilm ($MBEC_{50}$ = 0.029 nM) than triclosan ($MBEC_{50}$ = 10,784 nM) ($p < 0.0001$, Welch's *t*-test) (Figure 5B). In addition, GNR/Alg/PDADMAC also showed 186,469-fold higher potency in the eradication of the MSSA biofilm

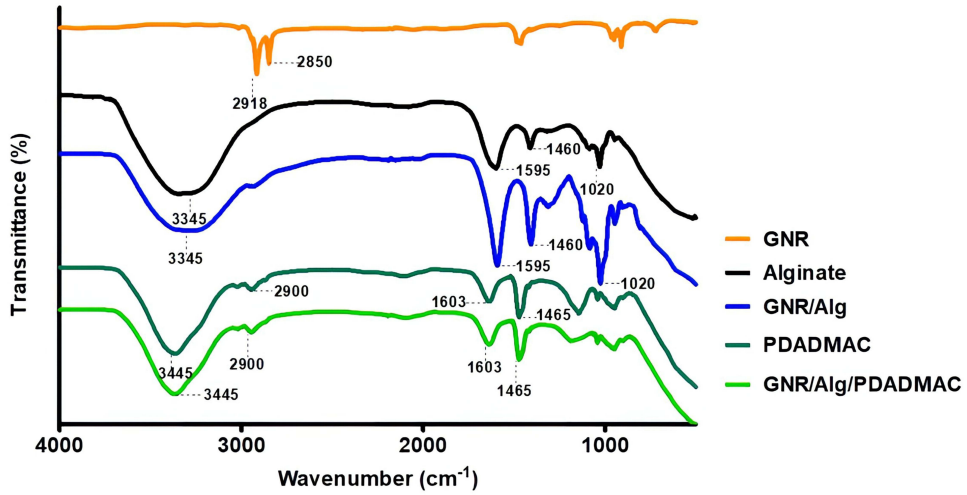

Figure 3 FTIR spectrum of non-coated gold nanorod (GNR), alginate, alginate-coated gold nanorod (GNR/Alg), PDADMAC and PDADMAC/alginate-coated gold nanorod (GNR/Alg/PDADMAC).

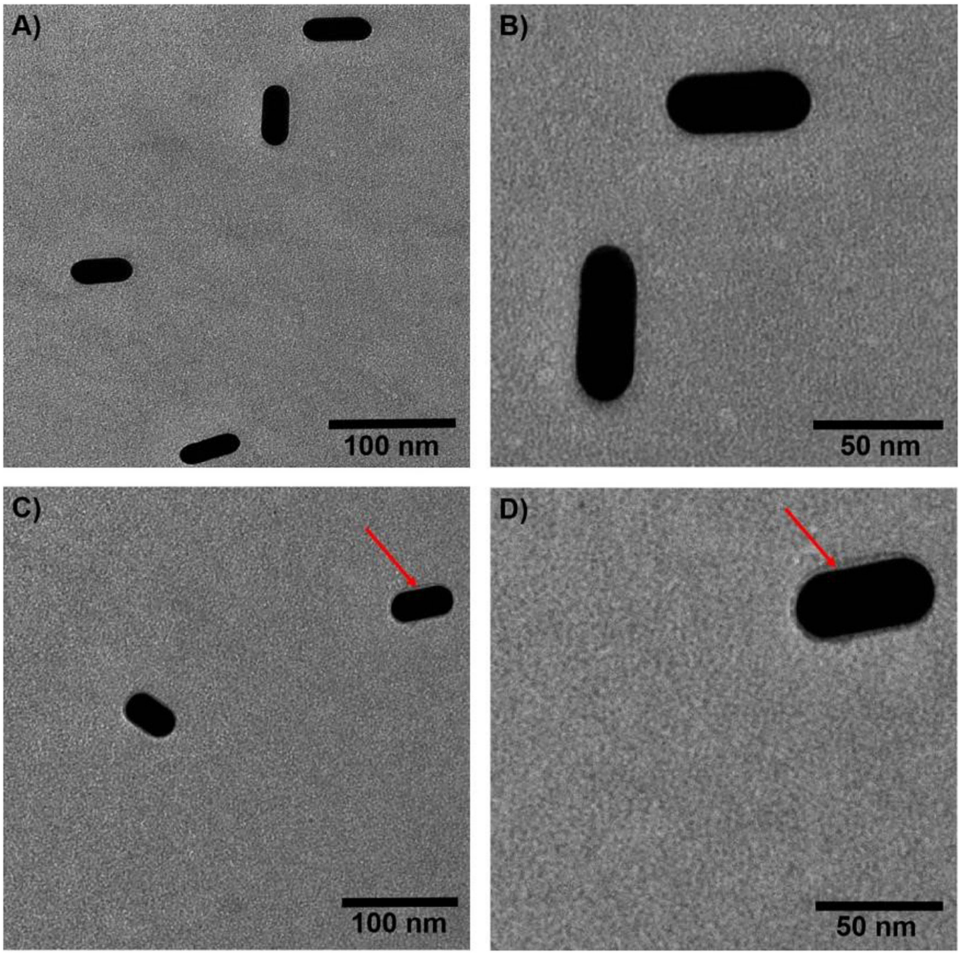

Figure 4 TEM micrographs of (**A**) non-coated gold nanorod (GNR) at 80,000× magnification (scale bar = 100 nm). (**B**) Enlarged inset of (**A**) (scale bar = 50 nm). (**C**) PDADMAC/alginate-coated gold nanorod (GNR/Alg/PDADMAC) at a concentration of 0.15 nM at magnification of 80,000× (scale bar = 100 nm). (**D**) Enlarged inset of (**C**) (scale bar = 50 nm). The red arrows indicate the faint layer of polyelectrolyte coating surrounding the GNR.

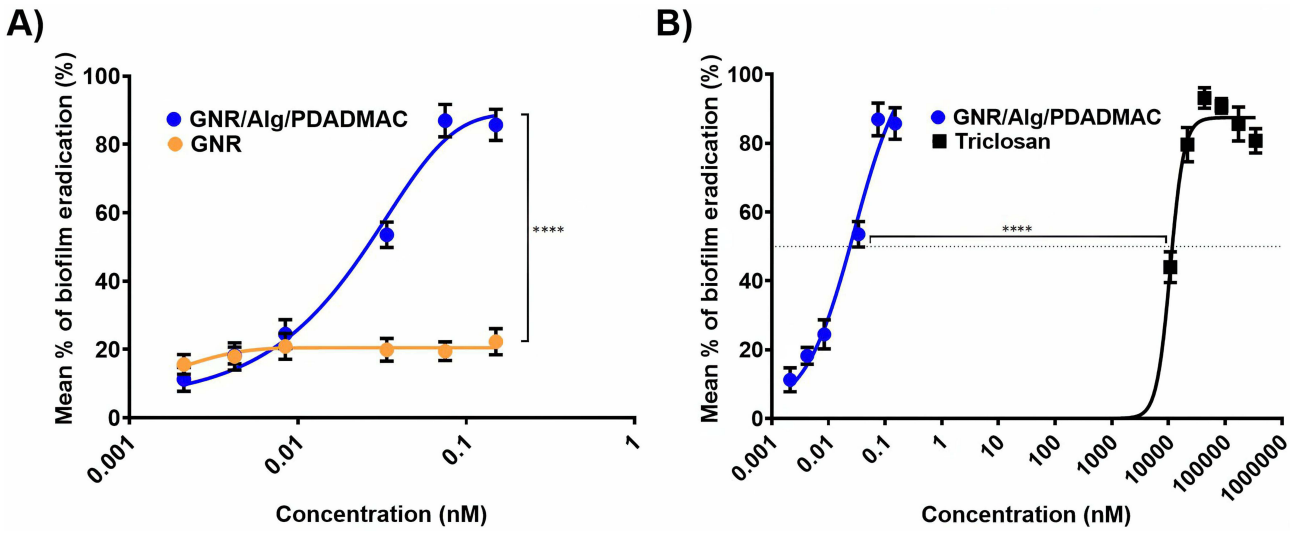

Figure 5 PDADMAC/alginate-coated gold nanorod (GNR/Alg/PDADMAC) showing (**A**) more efficient MRSA biofilm eradication (86% eradication at 0.15 nM GNR/Alg/PDADMAC) compared to non-coated gold nanorod (GNR, no significant biofilm eradication activities at 0.15 nM) (****$p < 0.0001$ at 0.15 nM, 2-way ANOVA - Bonferroni's multiple comparisons test) and (**B**) more potent MRSA biofilm eradication (50% eradication at 0.029 nM GNR/Alg/PDADMAC) compared to triclosan (50% eradication at 10,784 nM triclosan) (****$p < 0.0001$ at 50% eradication, Welch's *t*-test). Data are represented as mean ± SD (n = 3).

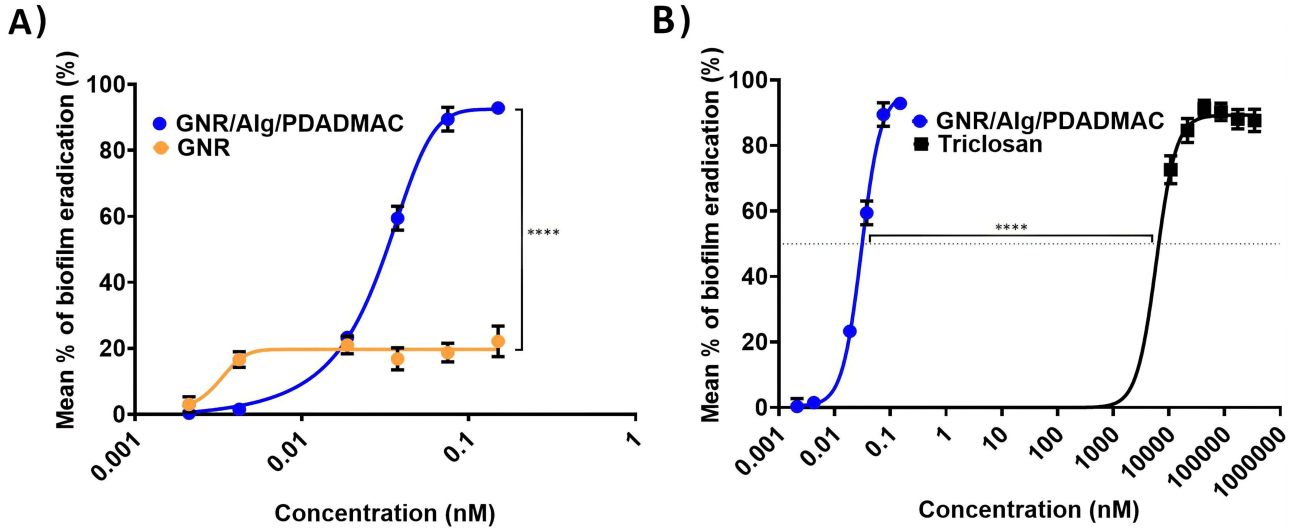

Figure 6 PDADMAC/alginate-coated gold nanorod (GNR/Alg/PDADMAC) showing (**A**) more efficient MSSA biofilm eradication (93% eradication at 0.15 nM GNR/Alg/PDADMAC) compared to non-coated gold nanorod (GNR, no significant biofilm eradication activities) (****$p < 0.0001$ at 0.15 nM, 2-way ANOVA - Bonferroni's multiple comparisons test) and (**B**) more potent MSSA biofilm eradication (50% eradication at 0.032 nM GNR/Alg/PDADMAC) than triclosan (50% eradication at 5967 nM triclosan) (****$p < 0.0001$ at 50% eradication, Welch's *t*-test). Data are represented as mean ± SD (n = 3).

($MBEC_{50}$ = 0.032 nM) when compared to that of the triclosan ($MBEC_{50}$ = 5967 nM) ($p < 0.0001$, Welch's *t*-test) (Figure 6B). The significant anti-biofilm properties of GNR/Alg/PDADMAC may be attributed to the polyelectrolyte coating, as shown by the absence of substantial dose-dependent biofilm eradication efficacies and potencies of the non-coated GNR in both the MRSA and MSSA biofilm models (Figures 5A and 6A). However, the polyelectrolyte alone, without GNR and with Alg coating, are ineffective in eradicating biofilms. The biofilm eradication curve for polyelectrolytes and GNR/Alg (intermediate nanoparticles during synthesis) presented in the Supplementary Section (Figure S1 and S5). The higher potency of GNR/Alg/PDADMAC in eradicating MRSA biofilm compared to the triclosan control may also reflect the inefficiency of triclosan in penetrating dense and complex MSSA biofilms for effective biofilm and microbial eradication.[57,58] This observation also suggests the ability of GNR/Alg/PDADMAC to penetrate and eradicate antimicrobial-resistant MRSA biofilms.

Time Point Assay

The progression of GNR/Alg/PDADMAC biofilm eradication was monitored using a time point assay. GNR/Alg/PDADMAC at 0.00015 µM (0.15 nM) eradicated 50% ($MBEC_{50}$) of MRSA and MSSA biofilm within 16.5 minutes (Figures 7A and S2) and 17 min (Figures 7B and S2), respectively. In contrast, triclosan (50 µM) destroyed 50% of the MRSA (Figure 7A) and MSSA (Figure 7B) biofilms within 12 and 16.5 minutes, respectively (Figure 7A and B). These results demonstrate that GNR/Alg/PDADMAC achieved comparable efficacy to triclosan at a 333,333-fold lower dosage, highlighting its potency in eradicating biofilms. Microscopic images of the biofilms are presented in the Supplementary Section (Figure S2).

FESEM

Untreated and GNR/Alg/PDADMAC-treated biofilms were further examined using FESEM. Both untreated MRSA and MSSA biofilms were intact and well established, as shown by the dense and overlapping bacterial cell aggregates within the biofilm at low magnification (5,000×) (Figure 8A and B). Under high magnification (20,000×) (Figure 8C and D), the bacterial cells appeared smooth with a typical round morphology. In contrast, treatment with GNR/Alg/PDADMAC induced significant disintegration of MRSA and MSSA biofilms, as shown by the major loss of biofilm and bacterial cell mass, arrangement of cells in short chains (Figure 8E and F), and alterations in cell morphology (denoted by the increase in cell surface roughness and abnormal cell shape) (Figures 8G and H). These findings are consistent with those of a previous biofilm eradication study[59] and demonstrate the biofilm eradication efficiency of GNR/Alg/PDADMAC.

CLSM

CLSM analysis was conducted on the MRSA and MSSA biofilms to investigate the effect of GNR/Alg/PDADMAC on the viability of the biofilm bacteria (Figure 9A), biofilm structure (Figure 9B), and biovolume (Figure 9D).[60] 2D CLSM analysis showed that GNR/Alg/PDADMAC treatment decreased the number of viable bacteria in MRSA and MSSA biofilms (Figure 9A), displaying significantly reduced green fluorescent staining. Figure 9C shows that GNR/Alg/PDADMAC caused a 5-fold reduction in the live/dead bacterial ratio compared to MRSA and MSSA growth controls (Figures 9C and D, $p < 0.0001$, 2-way ANOVA Bonferroni's multiple comparisons test). 3D CLSM analysis[61] further indicated that such a reduction may be associated with the loss of biofilm mass following GNR/Alg/PDADMAC treatment, as demonstrated by the loss of biofilm surface area, thickness and structured topography[62,63] (Figure 9B)

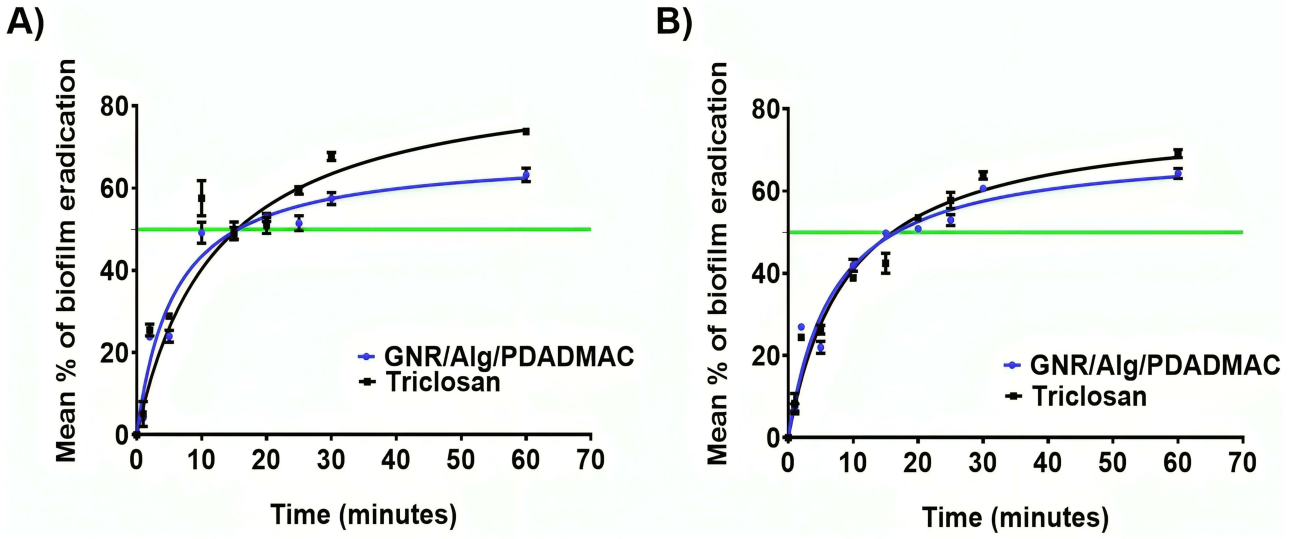

Figure 7 Time point assay for eradication of biofilms. (**A**) GNR/Alg/PDADMAC takes a slightly longer time (16.5 min) to achieve 50% MRSA biofilm eradication ($MBEC_{50}$) compared to triclosan (12 min) but at a significantly lower concentration (0.00015 µM GNR/Alg/PDADMAC vs 50 µM triclosan). Meanwhile, (**B**) GNR/Alg/PDADMAC takes a similar time span (17 min) to achieve 50% MSSA biofilm eradication ($MBEC_{50}$) compared to triclosan (16.5 min) but at a significantly lower concentration (0.00015 µM GNR/Alg/PDADMAC vs 50 µM triclosan). Green line indicates $MBEC_{50}$. Data are represented as mean ± SD (n = 3).

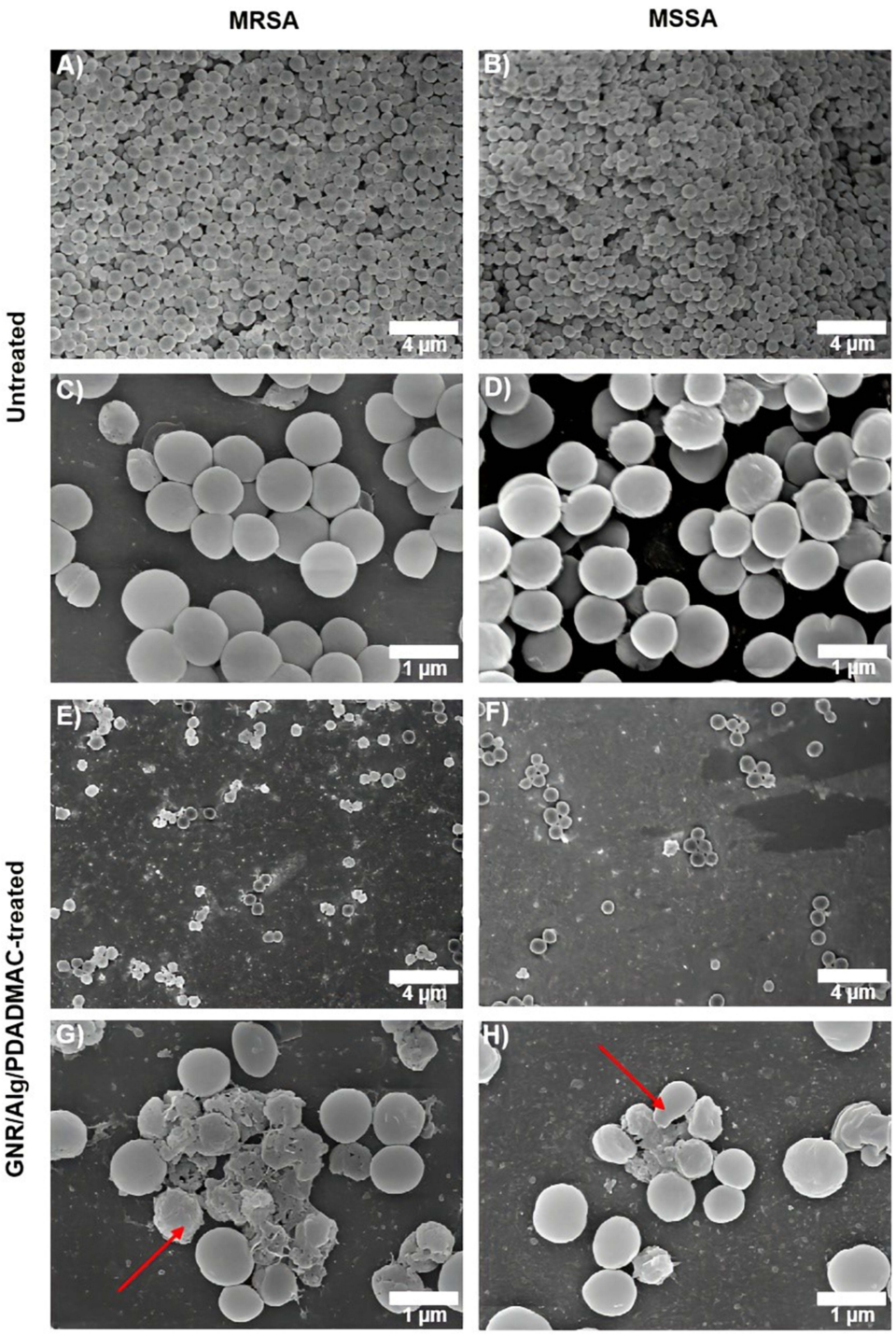

Figure 8 FESEM images of (**A**–**D**) untreated and (**E**–**H**) PDADMAC/alginate-coated gold nanorod (GNR/Alg/PDADMAC)-treated MRSA and MSSA biofilms under 5000× (scale bar = 4 µM) and 20,000× (Scale bar = 1 µM) magnification. The red arrows denote the alterations in cell morphology.

and biovolume[64] (Figure 9D shows ≥50% biovolume loss in both green (live bacteria) and red channels (dead bacteria)) in the MRSA and MSSA biofilms treated with GNR/Alg/PDADMAC when compared to that of the untreated groups (Figures 9B and D).

The CLSM results correlated with the FESEM findings, where GNR/Alg/PDADMAC dramatically decreased the number and thickness of biofilm cells (Figures 8 and 9). GNR/Alg/PDADMAC dramatically disrupted *S. aureus* biofilms (Figures 8E, F and 9A, B), whereas GNR/Alg/PDADMAC-treated *S. aureus* showed a complete absence of clumped

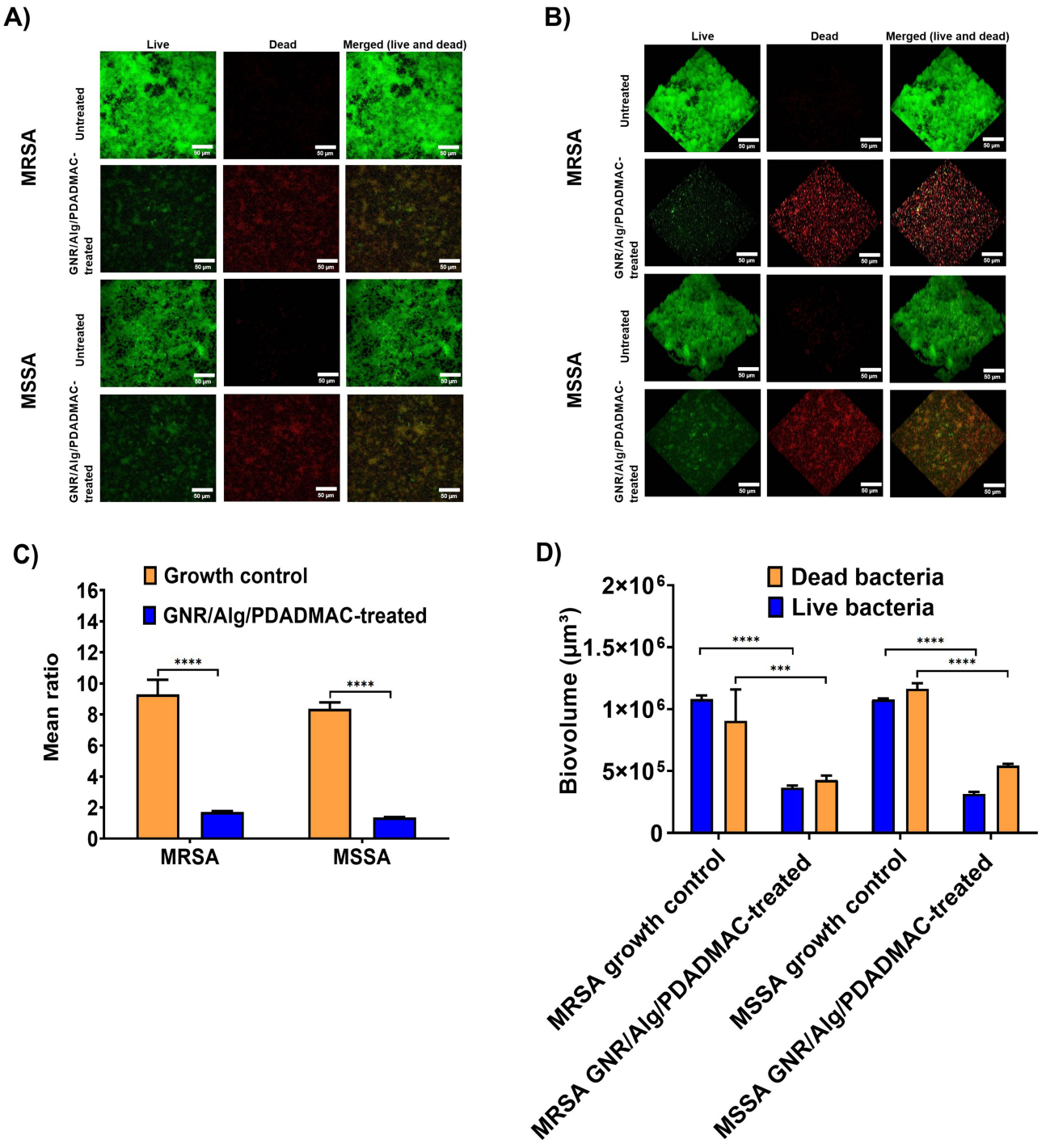

Figure 9 (**A**) Two-dimensional (2D) CLSM images of MRSA and MSSA strains under 40x magnification, manifesting the viability of both 0.03nM PDADMAC/alginate-coated gold nanorod (GNR/Alg/PDADMAC)-treated MRSA and MSSA biofilms were reduced significantly. (**B**) Three-dimensional (3D) CLSM images of MRSA and MSSA strains under 40x magnification. Both 0.03nM PDADMAC/alginate-coated gold nanorod (GNR/Alg/PDADMAC)-treated MRSA and MSSA biofilm structures were disrupted and reduced compared to their respective growth controls (Scale bar = 50 µM). (**C**) 0.03nM PDADMAC/alginate-coated gold nanorod (GNR/Alg/PDADMAC) treatment reduced the mean ratio of bacterial viability, as shown by the 5-fold reductions in the live: dead bacteria ratio of the PDADMAC/alginate-coated gold nanorod (GNR/Alg/PDADMAC) treatment groups (****: $p < 0.0001$, 2-way ANOVA - Bonferroni's multiple comparisons test). **(D)** Significant loss of biovolume was seen in MRSA and MSSA biofilms (***: $p < 0.001$, ****: $p < 0.0001$, 2-way ANOVA - Bonferroni's multiple comparisons test) after 0.03nM GNR/Alg/PDADMAC treatment (compared to growth controls). Data are represented as mean ± SD (n = 3).

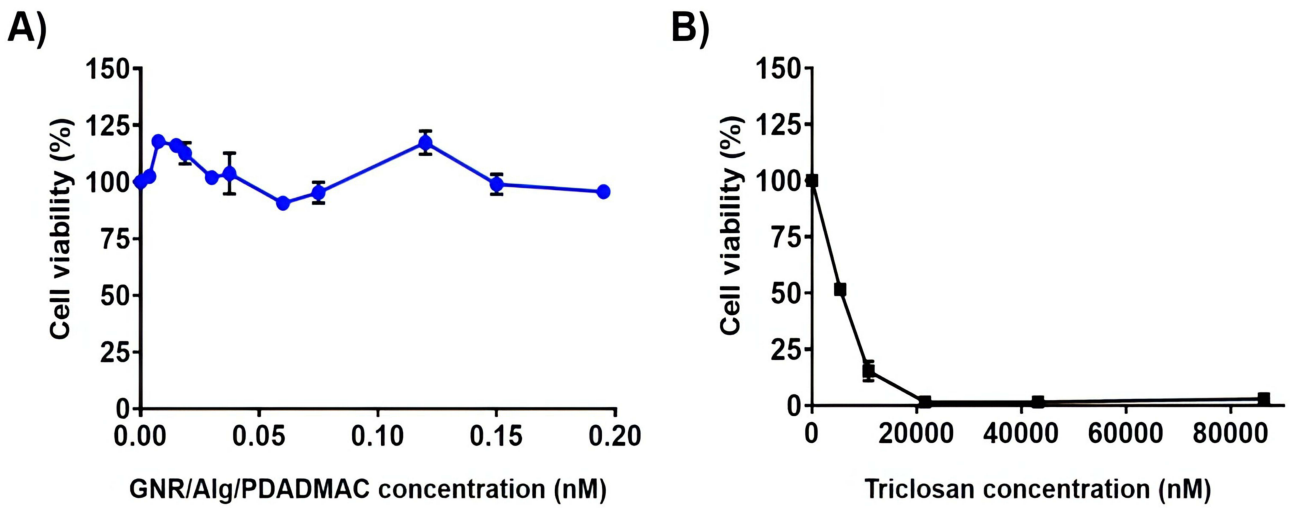

Figure 10 (**A**) PDADMAC/alginate-coated gold nanorod (GNR/Alg/PDADMAC) at a concentration range encompassing its biofilm eradication working concentrations did not cause significant death of L929 cells after 24 hours of incubation, suggesting good biocompatibility. (**B**) Triclosan at a concentration range encompassing its biofilm eradication working concentrations caused significant death of L929 cells after 24 hours of incubation. Data are represented as mean ± SD (n = 3).

cells in both FESEM (Figure 8E and F) and CLSM (Figure 9A and B). Moreover, in CLSM, the high red fluorescent staining in GNR/Alg/PDADMAC-treated MRSA and MSSA biofilms indicated dead bacteria with a disrupted cell membrane,[65] which was confirmed by FESEM analysis, where GNR/Alg/PDADMAC-treated MRSA and MSSA biofilms showed morphological changes (red arrows in Figure 8G and H).

Biocompatibility Assay

GNR/Alg/PDADMAC and triclosan's biocompatibilities were assessed on L929 murine fibroblast cells via MTT assay. GNR/Alg/PDADMAC was found to cause minimal toxicity to L929 cells at concentrations ranging from 0 to 0.2 nM (Figure 10A), which encompassed the maximum MRSA and MSSA biofilm eradication concentration (0.15 nM, Figures 5 and 6), with cell viability generally maintained above 90%. Triclosan caused toxicity to L929 cells, causing up to a 50% decrease in cell viability in the concentration range of 0–90.0 μM (Figure 10B), encompassing triclosan's maximum MRSA and MSSA biofilm eradication concentration (50.0 μM, Figures 5B and 6B). This suggests the biocompatibility of GNR/Alg/PDADMAC in the concentration range in which it exhibited effective biofilm eradication efficiency.

Discussion

Staphylococcus aureus biofilms are frequently associated with chronic infections and contamination of implantable medical devices.[66] In this work, we report the development of a PDADMAC/alginate-coated gold nanorod GNR/Alg/PDADMAC with an aspect ratio of 2.35 and zeta potential +42.80 ± 0.61 mV as an anti-biofilm agent that effectively removes established MRSA and MSSA biofilms from abiotic surfaces. Furthermore, the molar concentration of GNR/Alg/PDADMAC required to exert the same biofilm eradication potency ($MBEC_{50}$) was approximately 10^5 times lower in both MRSA and MSSA strains than the concentration of the positive control (triclosan) (Figures 5B and 6B).

PDADMAC-coated gold nanoparticles and gold nanorods have been previously investigated as potential agents for laser-induced photothermal (PTT) elimination of *S. aureus* and *E. coli*.[67] Nevertheless, these studies indicated that high gold nanoparticle concentrations (55.0 μg/mL) are required to generate significant photothermal effects for antibacterial purposes.[68] This may pose risks of heat-induced damage (emitted from high-concentration gold nanoparticles and light irradiation) to adjacent normal tissues during the process. In this study, we report the feasibility of using biocompatible GNR/Alg/PDADMAC directly to destroy MRSA and MSSA biofilms without photothermal activation. On the other hand, Figures S3 and S4 in the Supplementary Section demonstrated the GNR/Alg/PDADMAC and triclosan's biofilm eradication efficiency in gram-negative bacteria.

The effective MRSA and MSSA biofilm eradication by GNR/Alg/PDADMAC might be ascribed to their swift permeation through the biofilm via the water channels of the biofilm,[66,69] followed by the electrostatic interaction of the GNR/Alg/PDADMAC positively charged polyelectrolyte coating (Figure 2C) with the negatively charged lipoteichoic and teichoic acids of the gram-positive bacterial cell wall,[70] as well as the negatively charged components of the biofilm exopolysaccharide[56] matrix within the low-pH biofilm microenvironment.[39] Such interactions may decrease bacterial cell membrane integrity and cause subsequent cell membrane disintegration and loss of cell–cell or cell-EPS matrix association.[71] A similar phenomenon was observed in a previous study,[66] whereby *S. aureus* biofilms treated with AgNPs exhibited a similar FESEM morphology to that of the current study. Furthermore, the electrostatic interaction between GNR/Alg/PDADMAC and EPS may disrupt the integrity of the biofilm matrix (Figure 8E and F). This causes subsequent loss of bacterial and structural components from the biofilm.[64,72] The observations of the significant reduction in the number of viable biofilm bacteria and biofilm mass, and the disruption of the biofilm 3D structure following the GNR/Alg/PDADMAC treatment (Figures 9A–D) in the CLSM studies further supported this suggestion. Additionally, more CLSM images of the GNR/Alg/PDADMAC biofilm eradication were included in the Supplementary Part (Figure S6).

In this study, GNR/Alg/PDADMAC demonstrated better anti-biofilm effects, exerting 86% MRSA biofilm eradication and 93% MSSA eradication at a lower concentration, 0.15 nM GNR/Alg/PDADMAC, equivalent to 36.80 μg/mL when compared to non-coated GNR and other previously reported anti-biofilm nanoparticles. Most of the reported anti-biofilm nanoparticles exert anti-biofilm effects at higher concentrations. For example, positively charged AuNPs inhibited MSSA biofilm formation by 80% at 1 μM nanoparticle.[73] In comparison, curcumin-loaded hyperbranched polyethylenimine-grafted mesoporous silica nanoparticles (F-MSN-PEI/Cur) reduced biofilm bacterial viability and the mass of MRSA biofilms by >90% at 1600 μg/mL.[74] Meanwhile, zinc oxide nanoparticles maximally attenuated the formation of *E. coli* biofilms at 2791 μg/mL,[28] while magnesium oxide nanoparticles disrupted *Staphylococcus epidermidis* biofilm at 1.6 mg/mL.[29] In addition, 64 μg/mL of black phosphorus-conjugated gold nanoparticles inhibited the formation of *Enterococcus faecalis* biofilms by 33% and 58% in the absence and presence of near-infrared light, respectively.[74] In addition to metallic nanoparticles, *Lactobacillus gasseri* – originated biosurfactants loaded in liposomes – were also found to disperse >50% *S. aureus* biofilm at 2.5 mg/L.[75]

GNR/Alg/PDADMAC at a low working concentration (0.15 nM) was found to destroy 50% of the MRSA biofilm in vitro within a short interval (17 min) and achieve maximum biofilm eradication approximately 1 h after the initiation of incubation. In comparison, a higher concentration of triclosan (50 μM) was required to produce similar levels of MRSA biofilm eradication within a similar time frame. Similarly, the performance of GNR/Alg/PDADMAC was better than that of the standard antimicrobial agents. For instance, ciprofloxacin (100 μg/mL) required >5 h to disrupt 65% of *S. aureus* biofilm*s* in vitro, whereas daptomycin (200 μg/mL) and tobramycin (50 μg/mL) required approximately 10 h to disrupt 65% and 60% of *S. aureus* biofilms, respectively.

In this study, GNR/Alg/PDADMAC was more potent than triclosan based on a comparison of $MBEC_{50}$ values. Triclosan is commonly used to confront in-hospital *S. aureus* outbreaks and for topical decontamination of hospital patients colonised with MRSA.[76] Nevertheless, the widespread use of high concentrations of triclosan (as high as 8 μg/mL, higher than the concentration used in MRSA eradication baths)[77] for decontamination purposes in hospital settings has reduced MRSA susceptibility to triclosan[78] and raised chemical safety concerns.[79] In light of these results, GNR/Alg/PDADMAC was potent in disintegrating biofilms, affecting maximum biofilm disintegration at 0.15 a nanoparticle, of 36.80 μg/mL. Moreover, GNR/Alg/PDADMAC is biocompatible because it causes minimal toxicity to L929 cells, with cell viability maintained above 90% in the concentration range tested (0–0.2 nM), while disintegrating biofilms by electrostatic interaction-based cell membrane disintegration and disruption of cell–cell or cell-EPS matrix association, without harming normal tissue. Thus, GNR/Alg/PDADMAC offers potential as an effective and safe alternative biofilm eradication agent in hospital settings.

The GNR/Alg/PDADMAC may be formulated into irrigation solutions for cleaning infective wounds or biofilm-contaminated surfaces of medical apparatus that are attached to the patients and are difficult to clean, such as catheters, plastic tubing, and dental implants. According to the literature, if the surface of medical equipment is coated with a nanoparticle coating, the coating assists in resisting bacterial colonisation and subsequent biofilm growth on the medical devices.[80] It may also be formulated with existing antimicrobials to act synergistically by disintegrating biofilm layers and enabling the effective penetration of antibiotics into wounds and surfaces to disrupt biofilms and bacteria in the deeper regions of the wound or difficult-to-reach surfaces.

Further studies on GNR/Alg/PDADMAC, such as in vitro assessment of its biofilm eradication efficiency on different clinical-related surfaces, including catheters, plastic tubings, medical-implanted device surfaces, and additional bacterial species, its possible synergism with antibiotics, and in vivo assessment of its biofilm eradication efficiency in wounds (rat model) are currently in progress.

Conclusion

In summary, we successfully developed PDADMAC/alginate-coated gold nanorods (GNR/Alg/PDADMAC) that are biocompatible and more potent than triclosan in disintegrating MRSA and MSSA biofilms, possibly via electrostatic interactions with biofilm components. Such biofilm-eradicating nanoparticles may be effective agents for pathogenic biofilm eradication in the clinical setting.

Funding

This study was funded by an Impact-oriented Interdisciplinary Research Grant (IIRG) (project codes: IIRG003B-19FNW and IIRG003C-19FNW) from the Universiti Malaya and the Ministry of Higher Education, Malaysia. This work was supported in part by the National Science and Technology Council (NSTC), Taiwan, ROC. (NSTC 112-2321-B-A49-005, NSTC 111-2112-M-A49-025, MSTC 110-2923-M-009-005-MY3, NSTC 111-2927-I-A49-004, and NSTC 112-2927-I-A49-001), and the Ministry of Education through the SPROUT Project and the Center for Intelligent Drug Systems and Smart Biodevices (IDS^{2}B) of NYCU, Taiwan, ROC. Taiwan-Malaysia Semiconductor and Biomedical Oversea Science and Research Innovation Center, National Yang Ming Chiao Tung University, Hsinchu, Taiwan, ROC, for CCC.

Disclosure

Dr Sek Peng Chin reports a patent UI 2022007566, Malaysian Utility Innovation pending. Professor Lik Voon Kiew reports a patent UI 2022007566 pending. The authors report no other conflicts of interest in this work.

References

1. Piechota M, Kot B, Frankowska-Maciejewska A, Grużewska A, Woźniak-Kosek A. Biofilm formation by methicillin-resistant and methicillin-sensitive Staphylococcus aureus strains from hospitalized patients in Poland. *Biomed Res Int*. 2018;2018:1.
2. Chen C-J, Huang Y-C. New epidemiology of Staphylococcus aureus infection in Asia. *Clin Microbiol Infect*. 2014;20(7):605–623. doi:10.1111/1469-0691.12705
3. Lebeaux D, Ghigo J-M, Beloin C. Biofilm-related infections: bridging the gap between clinical management and fundamental aspects of recalcitrance toward antibiotics. *Microbiol Mol Biol Rev*. 2014;78(3):510–543. doi:10.1128/MMBR.00013-14
4. Donlan RM, Costerton JW. Biofilms: survival mechanisms of clinically relevant microorganisms. *Clin Microbiol Rev*. 2002;15(2):167–193. doi:10.1128/CMR.15.2.167-193.2002
5. Macfarlane S, Dillon J. Microbial biofilms in the human gastrointestinal tract. *J Appl Microbiol*. 2007;102(5):1187–1196. doi:10.1111/j.1365-2672.2007.03287.x
6. Wingender J, Flemming H-C. Biofilms in drinking water and their role as reservoir for pathogens. *Internat J Hyg Enviro Health*. 2011;214(6):417–423. doi:10.1016/j.ijheh.2011.05.009
7. Davies D. Understanding biofilm resistance to antibacterial agents. *Nat Rev Drug Discov*. 2003;2(2):114–122. doi:10.1038/nrd1008
8. Costerton JW, Stewart PS, Greenberg EP. Bacterial biofilms: a common cause of persistent infections. *Science*. 1999;284(5418):1318–1322. doi:10.1126/science.284.5418.1318
9. Stewart PS, Davison WM, Steenbergen JN. Daptomycin rapidly penetrates a Staphylococcus epidermidis biofilm. *Antimicrob Agents Chemother*. 2009;53(8):3505–3507. doi:10.1128/AAC.01728-08
10. Singh R, Ray P, Das A, Sharma M. Penetration of antibiotics through Staphylococcus aureus and Staphylococcus epidermidis biofilms. *J Antimicrob Chemother*. 2010;65(9):1955–1958. doi:10.1093/jac/dkq257
11. Doroshenko N, Tseng BS, Howlin RP, et al. Extracellular DNA impedes the transport of vancomycin in Staphylococcus epidermidis biofilms preexposed to subinhibitory concentrations of vancomycin. *Antimicrob Agents Chemother*. 2014;58(12):7273–7282. doi:10.1128/AAC.03132-14
12. Siala W, Mingeot-Leclercq M-P, Tulkens PM, Hallin M, Denis O, Van Bambeke F. Comparison of the antibiotic activities of daptomycin, vancomycin, and the investigational fluoroquinolone delafloxacin against biofilms from Staphylococcus aureus clinical isolates. *Antimicrob Agents Chemother*. 2014;58(11):6385–6397. doi:10.1128/AAC.03482-14
13. Xie Z, Siddiqi N, Rubin EJ. Differential antibiotic susceptibilities of starved Mycobacterium tuberculosis isolates. *Antimicrob Agents Chemother*. 2005;49(11):4778–4780. doi:10.1128/AAC.49.11.4778-4780.2005
14. Mascio CT, Alder JD, Silverman JA. Bactericidal action of daptomycin against stationary-phase and nondividing Staphylococcus aureus cells. *Antimicrob Agents Chemother*. 2007;51(12):4255–4260. doi:10.1128/AAC.00824-07
15. Dörr T, Vulić M, Lewis K. Ciprofloxacin causes persister formation by inducing the TisB toxin in Escherichia coli. *PLoS Biol*. 2010;8(2):e1000317. doi:10.1371/journal.pbio.1000317

16. Kwan BW, Valenta JA, Benedik MJ, Wood TK. Arrested protein synthesis increases persister-like cell formation. *Antimicrob Agents Chemother*. 2013;57(3):1468–1473. doi:10.1128/AAC.02135-12
17. Hengzhuang W, Wu H, Ciofu O, Song Z, Høiby N. In vivo pharmacokinetics/pharmacodynamics of colistin and imipenem in Pseudomonas aeruginosa biofilm infection. *Antimicrob Agents Chemother*. 2012;56(5):2683–2690. doi:10.1128/AAC.06486-11
18. Marquès C, Tasse J, Pracros A, et al. Effects of antibiotics on biofilm and unattached cells of a clinical Staphylococcus aureus isolate from bone and joint infection. *J Med Microbiol*. 2015;64(9):1021–1026. doi:10.1099/jmm.0.000125
19. Kiedrowski MR, Horswill AR. New approaches for treating staphylococcal biofilm infections. *Ann NY Acad Sci*. 2011;1241(1):104–121. doi:10.1111/j.1749-6632.2011.06281.x
20. Olson ME, Ceri H, Morck DW, Buret AG, Read RR. Biofilm bacteria: formation and comparative susceptibility to antibiotics. *Can J Vet Res*. 2002;66(2):86.
21. Choo EJ, Chambers HF. Treatment of methicillin-resistant Staphylococcus aureus bacteremia. *Infect Chemoth*. 2016;48(4):267–273. doi:10.3947/ic.2016.48.4.267
22. Karimaei S, Aghamir SMK, Foroushani AR, Pourmand MR. Antibiotic tolerance in biofilm persister cells of Staphylococcus aureus and expression of toxin-antitoxin system genes. *Microb Pathogenesis*. 2021;159:105126. doi:10.1016/j.micpath.2021.105126
23. John A-K, Baldoni D, Haschke M, et al. Efficacy of daptomycin in implant-associated infection due to methicillin-resistant Staphylococcus aureus: importance of combination with rifampin. *Antimicrob Agents Chemother*. 2009;53(7):2719–2724. doi:10.1128/AAC.00047-09
24. Tang H-J, Chen -C-C, Cheng K-C, et al. In vitro efficacy of fosfomycin-containing regimens against methicillin-resistant Staphylococcus aureus in biofilms. *J Antimicrob Chemother*. 2012;67(4):944–950. doi:10.1093/jac/dkr535
25. Tang H-J, Chen -C-C, Cheng K-C, et al. In vitro efficacies and resistance profiles of rifampin-based combination regimens for biofilm-embedded methicillin-resistant Staphylococcus aureus. *Antimicrob Agents Chemother*. 2013;57(11):5717–5720. doi:10.1128/AAC.01236-13
26. Khan ST, Ahamed M, Al-Khedhairy A, Musarrat J. Biocidal effect of copper and zinc oxide nanoparticles on human oral microbiome and biofilm formation. *Mater Lett*. 2013;97:67–70. doi:10.1016/j.matlet.2013.01.085
27. Agarwala M, Choudhury B, Yadav R. Comparative study of antibiofilm activity of copper oxide and iron oxide nanoparticles against multidrug resistant biofilm forming uropathogens. *Ind J Microbiol*. 2014;54:365–368. doi:10.1007/s12088-014-0462-z
28. Shakerimoghaddam A, Ghaemi EA, Jamalli A. Zinc oxide nanoparticle reduced biofilm formation and antigen 43 expressions in uropathogenic Escherichia coli. *Iran J Basic Med Sci*. 2017;20(4):451. doi:10.22038/IJBMS.2017.8589
29. Nguyen N-YT, Grelling N, Wetteland CL, Rosario R, Liu H. Antimicrobial activities and mechanisms of magnesium oxide nanoparticles (nMgO) against pathogenic bacteria, yeasts, and biofilms. *Sci Rep*. 2018;8(1):16260. doi:10.1038/s41598-018-34567-5
30. Hayat S, Muzammil S, Rasool MH, et al. In vitro antibiofilm and anti-adhesion effects of magnesium oxide nanoparticles against antibiotic resistant bacteria. *Microbiol Immunol*. 2018;62(4):211–220. doi:10.1111/1348-0421.12580
31. Rajkumari J, Magdalane CM, Siddhardha B, et al. Synthesis of titanium oxide nanoparticles using Aloe barbadensis mill and evaluation of its antibiofilm potential against Pseudomonas aeruginosa PAO1. *J Photochem Photobiol B Biol*. 2019;201:111667. doi:10.1016/j.jphotobiol.2019.111667
32. Jayaseelan C, Rahuman AA, Roopan SM, et al. Biological approach to synthesize TiO2 nanoparticles using Aeromonas hydrophila and its antibacterial activity. *Spectroch Acta Part A*. 2013;107:82–89. doi:10.1016/j.saa.2012.12.083
33. Khan ST, Ahamed M, Musarrat J, Al-Khedhairy AA. Anti-biofilm and antibacterial activities of zinc oxide nanoparticles against the oral opportunistic pathogens R othia dentocariosa and R othia mucilaginosa. *Europ J Oral Sci*. 2014;122(6):397–403. doi:10.1111/eos.12152
34. Dhandapani P, Maruthamuthu S, Rajagopal G. Bio-mediated synthesis of TiO2 nanoparticles and its photocatalytic effect on aquatic biofilm. *J Photochem Photobiol B Biol*. 2012;110:43–49. doi:10.1016/j.jphotobiol.2012.03.003
35. Shah RR, Kaewgun S, Lee BI, Tzeng T-RJ. The antibacterial effects of biphasic brookite-anatase titanium dioxide nanoparticles on multiple-drug-resistant Staphylococcus aureus. *J Biom Nanotechnol*. 2008;4(3):339–348. doi:10.1166/jbn.2008.324
36. Yang Z, Xie C. Zn2+ release from zinc and zinc oxide particles in simulated uterine solution. *Colloids Surf B*. 2006;47(2):140–145. doi:10.1016/j.colsurfb.2005.12.007
37. Macomber L, Imlay JA. The iron-sulfur clusters of dehydratases are primary intracellular targets of copper toxicity. *Proc Natl Acad Sci*. 2009;106(20):8344–8349. doi:10.1073/pnas.0812808106
38. Lee M-S, Hussein HR, Chang S-W, et al. Nature-inspired surface structures design for antimicrobial applications. *Int J Mol Sci*. 2023;24(2):1348. doi:10.3390/ijms24021348
39. Kawabata N, Takagishi K, Nishiguchi M. Coagulation and sedimentation of microbial cells by soluble pyridinium-type polymers. *Reactive Polymers*. 1989;10(2–3):269–273. doi:10.1016/0923-1137(89)90033-X
40. Brown S, Santa Maria JP, Walker S. Wall teichoic acids of gram-positive bacteria. *Ann Rev Microbiol*. 2013;67:313–336. doi:10.1146/annurev-micro-092412-155620
41. Nikoobakht B, El-Sayed MA. Preparation and growth mechanism of gold nanorods (NRs) using seed-mediated growth method. *Chem Mater*. 2003;15(10):1957–1962. doi:10.1021/cm020732l
42. Orendorff CJ, Murphy CJ. Quantitation of metal content in the silver-assisted growth of gold nanorods. *J Phys Chem A*. 2006;110(9):3990–3994. doi:10.1021/jp0570972
43. Bello V, Mattei G, Mazzoldi P, et al. Transmission electron microscopy of lipid vesicles for drug delivery: comparison between positive and negative staining. *Microsc Microanal*. 2010;16(4):456–461. doi:10.1017/S1431927610093645
44. Stepanović S, Vuković D, Hola V, et al. Quantification of biofilm in microtiter plates: overview of testing conditions and practical recommendations for assessment of biofilm production by staphylococci. *Apmis*. 2007;115(8):891–899. doi:10.1111/j.1600-0463.2007.apm_630.x
45. Jones GL, Muller C, O'reilly M, Stickler D. Effect of triclosan on the development of bacterial biofilms by urinary tract pathogens on urinary catheters. *J Antimicrob Chemother*. 2006;57(2):266–272. doi:10.1093/jac/dki447
46. Gilbert P, McBain AJ. Literature-based evaluation of the potential risks associated with impregnation of medical devices and implants with triclosan. *Surg Infect*. 2002;3(S1):s55–s63. doi:10.1089/sur.2002.3.s1-55
47. Reisner A, Krogfelt KA, Klein BM, Zechner EL, Molin S. In vitro biofilm formation of commensal and pathogenic Escherichia coli strains: impact of environmental and genetic factors. *J Bacteriol*. 2006;188(10):3572–3581. doi:10.1128/JB.188.10.3572-3581.2006
48. Beishenaliev A, Faruqu FN, Leo BF, et al. Facile synthesis of biocompatible sub-5 nm alginate-stabilised gold nanoparticles with sonosensitising properties. *Colloids Surf A*. 2021;627:127141. doi:10.1016/j.colsurfa.2021.127141

49. Kumar R, Binetti L, Nguyen TH, et al. Determination of the aspect-ratio distribution of gold nanorods in a colloidal solution using UV-visible absorption spectroscopy. *Sci Rep*. 2019;9(1):17469. doi:10.1038/s41598-019-53621-4
50. Mulvaney P. Surface plasmon spectroscopy of nanosized metal particles. *Langmuir*. 1996;12(3):788–800. doi:10.1021/la9502711
51. Gittins DI, Caruso F. Tailoring the polyelectrolyte coating of metal nanoparticles. *J Phys Chem A*. 2001;105(29):6846–6852. doi:10.1021/jp0111665
52. Wijaya A, Hamad-Schifferli K. Ligand customization and DNA functionalization of gold nanorods via round-trip phase transfer ligand exchange. *Langmuir*. 2008;24(18):9966–9969. doi:10.1021/la8019205
53. Barbosa JA, Abdelsadig MS, Conway BR, Merchant HA. Using zeta potential to study the ionisation behaviour of polymers employed in modified-release dosage forms and estimating their pKa. *Int J Pharm X*. 2019;1:100024.
54. Qiao Z, Yao Y, Song S, et al. Gold nanorods with surface charge-switchable activities for enhanced photothermal killing of bacteria and eradication of biofilm. *J Mat Chem B*. 2020;8(15):3138–3149. doi:10.1039/D0TB00298D
55. Palo E, Zhang H, Lastusaari M, Salomäki M. Nanometer-thick ion-selective polyelectrolyte multilayer coatings to inhibit the disintegration of inorganic upconverting nanoparticles. *ACS Appl Nano Mater*. 2020;3(7):6892–6898. doi:10.1021/acsanm.0c01245
56. Al-Khatib O, Böttcher C, von Berlepsch H, et al. Adsorption of polyelectrolytes onto the oppositely charged surface of tubular J-aggregates of a cyanine dye. *Colloid Polym Sci*. 2019;297:729–739. doi:10.1007/s00396-019-04487-5
57. Senobar Tahaei SA, Stájer A, Barrak I, Ostorházi E, Szabó D, Gajdács M. Correlation between biofilm-formation and the antibiotic resistant phenotype in Staphylococcus aureus isolates: a laboratory-based study in Hungary and a review of the literature. *Infect Drug Resist*. 2021;1155–1168. doi:10.2147/IDR.S303992
58. El-Azizi M, Rao S, Kanchanapoom T, Khardori N. In vitro activity of vancomycin, quinupristin/dalfopristin, and linezolid against intact and disrupted biofilms of staphylococci. *Ann Clinic Microbiol Antimicrob*. 2005;4(1):1–9. doi:10.1186/1476-0711-4-2
59. Bhattacharyya P, Agarwal B, Goswami M, Maiti D, Baruah S, Tribedi P. Zinc oxide nanoparticle inhibits the biofilm formation of Streptococcus pneumoniae. *Antonie Van Leeuwenhoek*. 2018;111:89–99. doi:10.1007/s10482-017-0930-7
60. Guilbaud M, Piveteau P, Desvaux M, Brisse S, Briandet R. Exploring the diversity of Listeria monocytogenes biofilm architecture by high-throughput confocal laser scanning microscopy and the predominance of the honeycomb-like morphotype. *Appl Environ Microbiol*. 2015;81(5):1813–1819. doi:10.1128/AEM.03173-14
61. Bridier A, Dubois-Brissonnet F, Boubetra A, Thomas V, Briandet R. The biofilm architecture of sixty opportunistic pathogens deciphered using a high throughput CLSM method. *J Microbiol Methods*. 2010;82(1):64–70. doi:10.1016/j.mimet.2010.04.006
62. Akiyama H, Hamada T, Huh WK, et al. Confocal laser scanning microscopic observation of glycocalyx production by Staphylococcus aureus in skin lesions of bullous impetigo, atopic dermatitis and pemphigus foliaceus. *Br J Dermatol*. 2003;148(3):526–532. doi:10.1046/j.1365-2133.2003.05162.x
63. Buzón-Durán L, Alonso-Calleja C, Riesco-Peláez F, Capita R. Effect of sub-inhibitory concentrations of biocides on the architecture and viability of MRSA biofilms. *Food Microbiol*. 2017;65:294–301. doi:10.1016/j.fm.2017.01.003
64. Desroche N, Dropet C, Janod P, Guzzo J. Antibacterial properties and reduction of MRSA biofilm with a dressing combining polyabsorbent fibres and a silver matrix. *J Wound Care*. 2016;25(10):577–584. doi:10.12968/jowc.2016.25.10.577
65. Li J, Zhong W, Zhang K, Wang D, Hu J, Chan-Park MB. Biguanide-derived polymeric nanoparticles kill MRSA biofilm and suppress infection in vivo. *ACS Appl Mater Interfaces*. 2020;12(19):21231–21241. doi:10.1021/acsami.9b17747
66. Ansari M, Khan H, Khan A, Cameotra S, Alzohairy M. Anti-biofilm efficacy of silver nanoparticles against MRSA and MRSE isolated from wounds in a tertiary care hospital. *Indian J Med Microbiol*. 2015;33(1):101–109. doi:10.4103/0255-0857.148402
67. Zhang R, Yu J, Ma K, Ma Y, Wang Z. Synergistic chemo-photothermal antibacterial effects of polyelectrolyte-functionalized gold nanomaterials. *ACS Appl Bio Mater*. 2020;3(10):7168–7177. doi:10.1021/acsabm.0c00979
68. Hu D, Li H, Wang B, et al. Surface-adaptive gold nanoparticles with effective adherence and enhanced photothermal ablation of methicillin-resistant Staphylococcus aureus biofilm. *ACS Nano*. 2017;11(9):9330–9339. doi:10.1021/acsnano.7b04731
69. Kalishwaralal K, BarathManiKanth S, Pandian SRK, Deepak V, Gurunathan S. Silver nanoparticles impede the biofilm formation by Pseudomonas aeruginosa and Staphylococcus epidermidis. *Colloids Surf B*. 2010;79(2):340–344. doi:10.1016/j.colsurfb.2010.04.014
70. Pajerski W, Ochonska D, Brzychczy-Wloch M, et al. Attachment efficiency of gold nanoparticles by Gram-positive and Gram-negative bacterial strains governed by surface charges. *J Nanopart Res*. 2019;21:1–12. doi:10.1007/s11051-019-4617-z
71. Masurkar S, Chaudhari P, Shidore V, Kamble S. Effect of biologically synthesised silver nanoparticles on Staphylococcus aureus biofilm quenching and prevention of biofilm formation. *IET Nanobiotechnol*. 2012;6(3):110–114. doi:10.1049/iet-nbt.2011.0061
72. Alavi M, Stojadinovic A, Zao M. An overview of biofilm and its detection in clinical samples. *J Wound Care*. 2012;21(8):376–383. doi:10.12968/jowc.2012.21.8.376
73. Giri K, Yepes LR, Duncan B, et al. Targeting bacterial biofilms via surface engineering of gold nanoparticles. *RSC Adv*. 2015;5(128):105551–105559. doi:10.1039/C5RA16305F
74. Pamukçu A, Erdoğan N, Şen Karaman D. Polyethylenimine-grafted mesoporous silica nanocarriers markedly enhance the bactericidal effect of curcumin against Staphylococcus aureus biofilm. *J Biomed Mater Res Part B*. 2022;110(11):2506–2520. doi:10.1002/jbm.b.35108
75. Giordani B, Costantini PE, Fedi S, et al. Liposomes containing biosurfactants isolated from Lactobacillus gasseri exert antibiofilm activity against methicillin resistant Staphylococcus aureus strains. *Eur J Pharm Biopharm*. 2019;139:246–252. doi:10.1016/j.ejpb.2019.04.011
76. Al-Doori Z, Morrison D, Philpott-Howard J. Small colony variants and triclosan resistance in five international clones of methicillin resistant Staphylococcus aureus. *J Mol Bio Res*. 2017;7(1):112. doi:10.5539/jmbr.v7n1p112
77. Bamber A, Neal T. An assessment of triclosan susceptibility in methicillin-resistant and methicillin-sensitive Staphylococcus aureus. *J Hosp Infect*. 1999;41(2):107–109. doi:10.1016/S0195-6701(99)90047-6
78. Ciusa ML, Furi L, Knight D, et al. A novel resistance mechanism to triclosan that suggests horizontal gene transfer and demonstrates a potential selective pressure for reduced biocide susceptibility in clinical strains of Staphylococcus aureus. *Int J Antimicrob Agents*. 2012;40(3):210–220. doi:10.1016/j.ijantimicag.2012.04.021
79. Forbes S, Latimer J, Bazaid A, McBain AJ. Altered competitive fitness, antimicrobial susceptibility, and cellular morphology in a triclosan-induced small-colony variant of Staphylococcus aureus. *Antimicrob Agents Chemother*. 2015;59(8):4809–4816. doi:10.1128/AAC.00352-15
80. Knetsch ML, Koole LH. New strategies in the development of antimicrobial coatings: the example of increasing usage of silver and silver nanoparticles. *Polymers*. 2011;3(1):340–366. doi:10.3390/polym3010340